


RESEARCH ARTICLE

Open Access



# Antagonistic effects of mitochondrial matrix and intermembrane space proteases on yeast aging

Montserrat Vega<sup>1</sup>, David Castillo<sup>2</sup>, Laura de Cubas<sup>1</sup>, Yirong Wang<sup>3</sup>, Ying Huang<sup>3</sup>, Elena Hidalgo<sup>1</sup> and Margarita Cabrera<sup>1,4\*</sup> 

## Abstract

**Background:** In many organisms, aging is characterized by a loss of mitochondrial homeostasis. Multiple factors such as respiratory metabolism, mitochondrial fusion/fission, or mitophagy have been linked to cell longevity, but the exact impact of each one on the aging process is still unclear.

**Results:** Using the deletion mutant collection of the fission yeast *Schizosaccharomyces pombe*, we have developed a genome-wide screening for mutants with altered chronological lifespan. We have identified four mutants associated with proteolysis at the mitochondria that exhibit opposite effects on longevity. The analysis of the respiratory activity of these mutants revealed a positive correlation between increased respiration rate and prolonged lifespan. We also found that the phenotype of the long-lived protease mutants could not be explained by impaired mitochondrial fusion/fission activities, but it was dependent on mitophagy induction. The anti-aging role of mitophagy was supported by the effect of a mutant defective in degradation of mitochondria, which shortened lifespan of the long-lived mutants.

**Conclusions:** Our characterization of the mitochondrial protease mutants demonstrates that mitophagy sustains the lifespan extension of long-lived mutants displaying a higher respiration potential.

**Keywords:** Chronological aging, Mitochondrial dynamics, Mitophagy, Mitoproteases, Respiratory capacity

## Background

With the growing elderly populations worldwide, increasing efforts have been focused on the study of aging-associated diseases and healthspan. Several biological processes have been linked with aging in different organisms. Among them, genomic instability, impaired proteostasis, and mitochondrial dysfunction constitute relevant hallmarks of aging [1].

In the last decades, numerous studies using yeast as a model system have contributed to our understanding of the aging process. Aging in yeast, like in many organisms, involves three basic features: reduced resistance to stresses, a decline in reproduction, and increased mortality. Moreover, calorie restriction, the most common anti-aging intervention, increases longevity in yeast and other model organisms including flies, nematodes, and mice [2]. The effect of calorie restriction is probably mediated by the inhibition of highly conserved nutrient-responsive kinases: TOR/SK6 and Ras/adenylate cyclase (AC)/PKA. Deletion of components of PKA and TOR pathways is known to induce lifespan extension in yeast through the activation of stress responses [3–5]. In the case of TOR

\*Correspondence: mcabrera@cblm.csic.es

<sup>1</sup>Oxidative Stress and Cell Cycle Group, Universitat Pompeu Fabra, C/ Dr. Aiguader 88, 08003 Barcelona, Spain  
Full list of author information is available at the end of the article



© The Author(s) 2022. **Open Access** This article is licensed under a Creative Commons Attribution 4.0 International License, which permits use, sharing, adaptation, distribution and reproduction in any medium or format, as long as you give appropriate credit to the original author(s) and the source, provide a link to the Creative Commons licence, and indicate if changes were made. The images or other third party material in this article are included in the article's Creative Commons licence, unless indicated otherwise in a credit line to the material. If material is not included in the article's Creative Commons licence and your intended use is not permitted by statutory regulation or exceeds the permitted use, you will need to obtain permission directly from the copyright holder. To view a copy of this licence, visit <http://creativecommons.org/licenses/by/4.0/>. The Creative Commons Public Domain Dedication waiver (<http://creativecommons.org/publicdomain/zero/1.0/>) applies to the data made available in this article, unless otherwise stated in a credit line to the data.

inhibition, autophagy is stimulated and could also contribute to lifespan extension [6].

Two versions of lifespan exist in yeast: replicative and chronological lifespan [7]. Replicative lifespan (RLS) is defined by the number of daughter cells produced by a single cell before senescence. This process is equivalent to the longevity of proliferating cells in higher multicellular organisms. Chronological lifespan (CLS) represents the viability of a yeast cell during the stationary phase and recapitulates aging of non-proliferating cells. RLS and CLS are tightly connected and mutant strains with decreased replicative potential often exhibit a limited CLS.

Most research in yeast aging has been conducted using the budding yeast *Saccharomyces cerevisiae* (for reviews, see [8, 9]) but lately the fission yeast *Schizosaccharomyces pombe* has emerged as a powerful and complementary chronological aging model. Respiratory metabolism plays a central role in the regulation of chronological aging. In *S. pombe*, mutations in components of the electron transport chain (ETC) cause elevated reactive oxygen species (ROS) levels and shortening of CLS [10]. Protection from ROS is essential to ensure normal CLS as revealed by a double mutant lacking superoxide dismutase and with low glutathione levels [11]. This mutant is more sensitive to oxidative stress and displays increased levels of protein oxidation and shorter CLS.

To avoid the accumulation of oxidized and damaged proteins, mitochondria contain their own protein quality control (PQC) system, which includes two basic components: chaperones and proteases [12]. In both yeast models, chaperones of the Hsp90, Hsp70, and Hsp60 families and small Hsp (sHsp) assist in protein folding or refolding steps whereas ATP-dependent proteases are responsible for protein maturation or degradation. Mitochondria of fission yeast contain three main proteases: one soluble localized at the matrix called Lon1 and two membrane proteases, Yme1 which has its catalytic domains facing the intermembrane space and Yta12 with catalytic domains oriented towards the matrix. Moreover, the yeast protein Mgr3 serves as an adaptor for the protease Yme1 during the recognition of its substrates [13].

Controlled mitochondrial dynamics represents a second quality control pathway linked with the process of aging. In *S. cerevisiae*, mitochondrial fragmentation and reduced membrane potential have been reported with increasing replicative age, although it is unclear whether these events contribute to senescence [14, 15]. Notably, chronologically aged cells of fission yeast show reduced mitochondrial signal and loss of tubular mitochondria compared to young cells [16]. In budding yeast, loss of the mitochondrial fission machinery causes increased RLS whereas the absence of Mgm1 involved in fusion has

been associated with shortening of RLS [17, 18]. Interestingly, a double mutant of *S. cerevisiae* with defective fusion and fission displays wild-type mitochondrial morphology, but decreased lifespan suggesting that the critical step in the control of lifespan is the balance between fusion and fission events and not the morphology [19].

A third strategy to ensure mitochondrial homeostasis is the removal of the organelle by mitophagy [20]. This process is initiated in the cytosol with the formation of a double-membrane structure (phagophore) that engulfs the damaged or superfluous mitochondria. After the sealing of the membrane around the organelle, the resulting autophagosome fuses with the lysosome (vacuole in yeast) where proteins and lipids are degraded. Most of the key components required in autophagy have been identified in budding yeast, including the receptor on the mitochondrial outer membrane (Atg32) recognized by the autophagy machinery [21]. Recently, two studies have also revealed the identity of specific components of the mitophagy pathway in fission yeast [22, 23].

Using the *S. pombe* deletion mutant collection, we have performed a genome-wide screening and identified four longevity mutants that are involved in mitochondrial protein quality control. While the absence of two proteases, Lon1 and Yta12, which reside in the matrix conferred a severe defect in CLS, mutant cells lacking the intermembrane space protease Yme1 and its adaptor protein Mgr3 were long-lived. The short-lived mutants displayed reduced oxygen consumption, low levels of mitochondrial DNA-encoded proteins, and impaired mitophagy, while the opposite characterized the long-lived mutants. Moreover, inhibition of mitophagy abolished the lifespan extension of both long-lived mutants implying that mitophagy is essential for delaying the aging process. On the other hand, we were not able to establish a direct connection between the longevity phenotypes and mitochondrial dynamics. In conclusion, the analysis of the mitochondrial function of these mutants reveals that increased respiratory potential and mitophagy act together to prolong lifespan by maintaining optimal mitochondrial function.

## Results

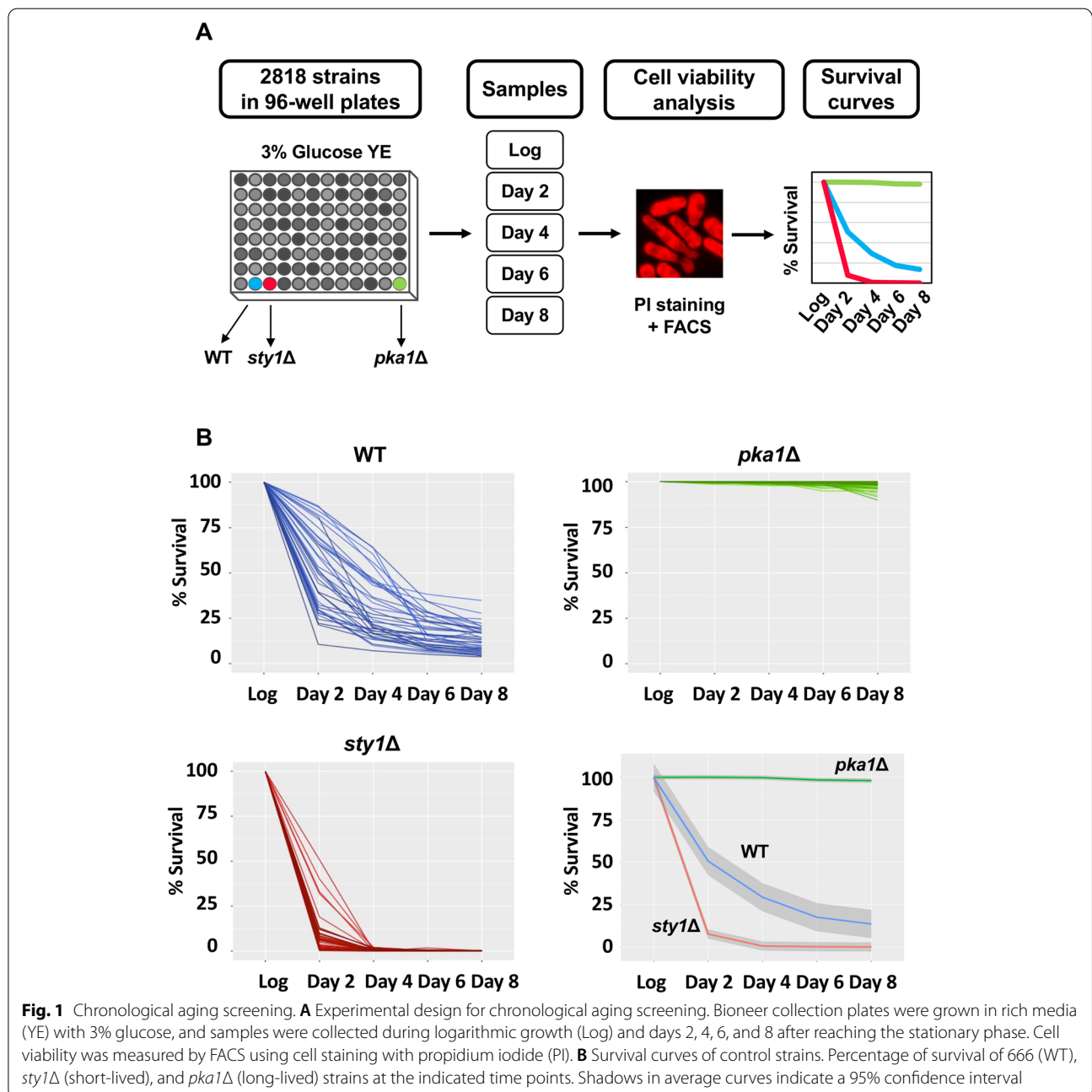
### Genome-wide screening for longevity deletion mutants in fission yeast

The classical method to monitor cell viability during chronological aging is based on the division potential of stationary phase cells when nutrients are replenished [7]. A possible caveat of this system is the identification of short-lived mutants that might be only affected in cell division, but not directly related to the aging process. To overcome this limitation, we have developed a genome-wide screening where cell viability is monitored

by the uptake of a fluorescent dye (propidium iodide, PI) and flow cytometry [24]. Only dead cells with enhanced membrane permeability will be stained with PI.

A total of 2818 deletion mutants (Bioneer collection version 2) were grown in 96-well plates in rich media containing 3% glucose (Fig. 1A, Additional file 1: Table S1). Each plate also included three control strains: wild type (WT), *sty1Δ* (short-lived), and *pka1Δ* (long-lived) [5, 25]. Both kinases, Sty1 and Pka1, are well-characterized by their function in stress response and nutrient signaling,

respectively. Every 2 days until day 8, cells from aged cultures were stained with PI and analyzed by flow cytometry to quantify the non-stained and viable population. The fraction of viable cells at each time point allowed us to represent the survival curve of each deletion mutant. Figure 1B shows the survival curves of wild type, *sty1Δ*, and *pka1Δ* from different plates or experiments and the average curve for each control strain, where short- or long-lived mutants can be clearly distinguished from wild-type cells.



### Around 500 deletion mutants display altered longevity in rich media

We chose the area under the survival curve as the ideal parameter to compare the longevity of the mutants and control strains (wild type, *sty1Δ*, and *pka1Δ*). We first obtained the area distribution of the control strains and used a Bayesian approximation to estimate the probability of each mutant to belong to the different distributions (Fig. 2A). The survival of most mutants reproduced the wild-type distribution, 163 were classified as short-lived mutants, and 309 were identified as long-lived mutants (Fig. 2B, Additional file 2: Table S2). The larger number of long-lived mutants could be explained by the growth in rich media, which favors the identification of those mutants that mimic lifespan extension by calorie restriction [5].

To highlight the biological processes with more impact on CLS, we performed a Gene Ontology (GO) enrichment analysis including all mutants with altered longevity. We identified a few enriched cellular components, which are involved in plasma membrane organization, oxidative stress response, and ribosome function (Fig. 2C, Additional file 3: Table S3). As expected, several biological processes that have been linked previously to aging, such as stress response, cell cycle progression, and protein quality control (PQC) were overrepresented (Fig. 2D, Additional file 3: Table S3). This last term (PQC for misfolded or incompletely synthesized proteins) caught our attention since it includes two genes coding for Lon1 and Mgr3, both involved in mitochondrial protein turnover, but with opposite longevity phenotypes. Lack of the mitochondrial protease Lon1 reduced longevity whereas the absence of Mgr3, adaptor protein of the protease Yme1 [13], led to increased lifespan. We chose to deepen into the analysis of these mutants, since their opposite phenotypes highlight the complexity of the effects of mitochondrial homeostasis in cell longevity.

### Cells lacking mitochondrial proteases are affected in their longevity profiles

To analyze the role of mitochondrial PQC in chronological aging, we decided to examine the longevity of another two mitoprotease mutants, *yme1Δ* and *yta12Δ*, which were missing in our deletion collection. Both

proteases form multimeric complexes localized in the inner mitochondrial membrane and contain conserved AAA+ domains for membrane extraction of their substrates. Yme1 and Yta12 are known as i-AAA and m-AAA proteases, respectively, because their catalytic domains are exposed to opposite sides of the inner mitochondrial membrane (Fig. 3A). As mentioned above, mitochondria in *S. pombe* hold a third ATP-dependent protease Lon1, which is localized in the matrix, and the adaptor protein Mgr3 acting together with Yme1 in the proteolysis of mitochondrial membrane proteins (Fig. 3A).

Using the flow cytometry-based assay and prototrophic strains, we recapitulated the opposite longevity phenotypes of *lon1Δ* and *mgr3Δ* mutants (Fig. 3B). Moreover, cells lacking the protease Yme1 displayed increased lifespan in a similar manner to *mgr3Δ* mutant, whereas the loss of the protease Yta12 resulted in a significant reduction of longevity (Fig. 3B). Next, we analyzed the viability of these four deletion mutants monitoring how cells resume growth after chronological aging. We performed the traditional assay, where aged cells from different time points (days 2–6) were spotted in rich media to allow growth (Fig. 3C). This alternative method confirmed the longevity phenotypes of the four mutants; *lon1Δ* and *yta12Δ* were classified as short-lived mutants whereas *mgr3Δ* and *yme1Δ* cells exhibited increased survival under chronological aging (Fig. 3C).

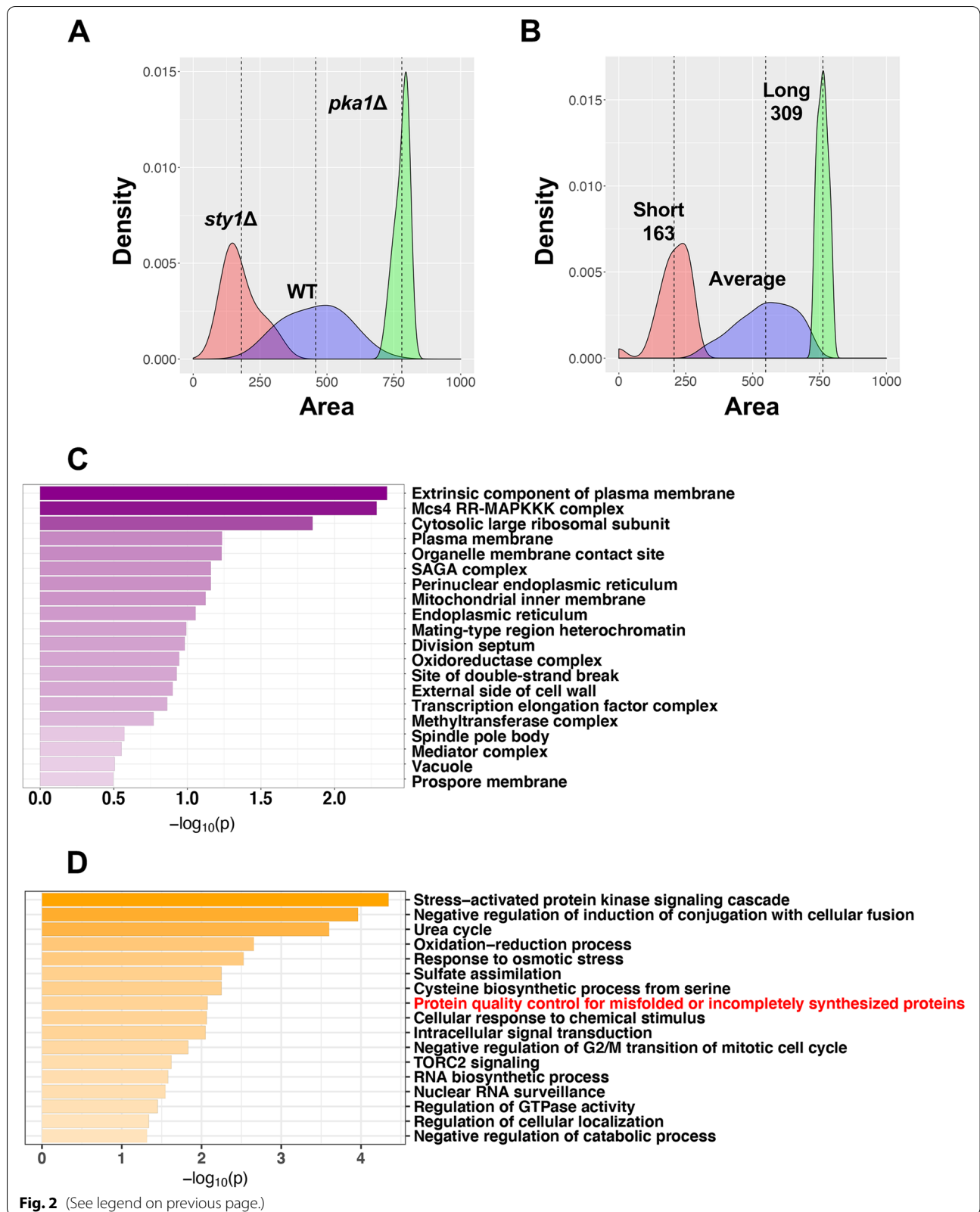
### The short- or long-lived protease mutants display decreased or enhanced respiratory rates, respectively

To better understand the possible functions of the mitochondrial proteases in aging, we focused on the analysis of the respiratory activity of the deletion mutants. We first examined the growth of the mutants in rich or minimal media with low glucose concentration (0.08% Glu) that promote respiratory metabolism (Fig. 4A). We observed that the short-lived mutants *lon1Δ* and *yta12Δ* showed a severe growth defect in respiratory-prone media, comparable to that detected in *cox6Δ* lacking a subunit of the ETC complex IV [5]. In contrast, long-lived mutants *mgr3Δ* and *yme1Δ* displayed a normal growth in low glucose conditions (Fig. 4A). In concordance with these results, when we monitored oxygen consumption of the mutants, cells lacking Lon1 or Yta12 displayed

(See figure on next page.)

**Fig. 2** Classification of chronological aging mutants and Gene Ontology (GO) enrichment analysis. **A, B** Area distribution of the control strains used in the screening. Density plot showing the survival distribution of the three control strains: 666 (WT), *sty1Δ* (short-lived strain), and *pka1Δ* (long-lived strain). These distributions were considered to estimate the probability for every analyzed mutant to belong to each one of these groups. Once these posterior probabilities were calculated, each mutant was assigned to the category with the highest probability. The density plot (**B**) shows the resulting classification of mutants based on this approach. **C, D** Gene Ontology term enrichment. The long-lived (309) and short-lived (163) mutants identified in the screening were selected for GO enrichment analysis. They were classified into Cellular Component (**C**) and Biological Process (**D**) GO terms using Metascape [64]. Each bar represents a GO term ordered by statistical significance ( $-\log_{10} p$  value)





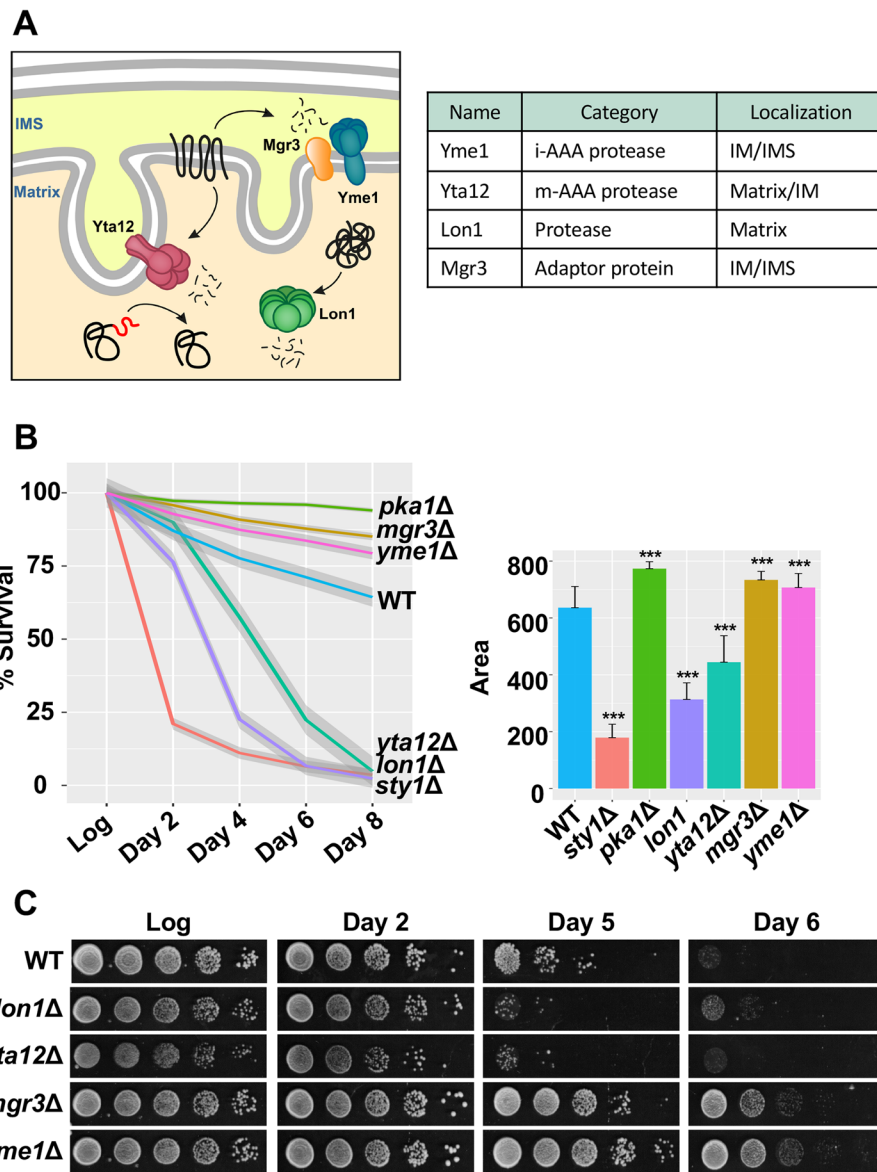


**Fig. 3** Deletion of mitochondrial proteases affects longevity. **A** Scheme and table depicting the localization of the mitochondrial proteases Lon1, Yta12, Yme1, and the adaptor protein Mgr3. **B, C** Deletion of the mitoproteases Lon1 or Yta12 decreases lifespan, whereas deletion of Mgr3 or Yme1 increases longevity. Strains 972 (WT), *lon1Δ*, *yta12Δ*, *mgr3Δ*, and *yme1Δ* were grown in rich media with 3% glucose and viability was measured by FACS using propidium iodide (**B**) and survival spots (**C**). **B** Line plot represents the local regression curves for the average survival of each strain ( $n > 30$ ) at different time points. Each survival curve also displays a 95% confidence interval band. Bar plot depicts the average area under the survival curve of each strain, and error bars represent SD. Significant differences between deletion strains and wild type were determined by two-sided *t*-test ( $*p < 0.05$ ,  $**p < 0.01$ ,  $***p < 0.001$ ). **C** Serial dilutions of culture samples from the logarithmic phase (Log) and days 2, 5, and 6 of the stationary phase were spotted onto rich media plates

decreased respiratory capacity in high and low glucose conditions whereas the loss of Mgr3 or Yme1 was associated with enhanced respiration (Fig. 4B). This increase in the respiratory activity was more evident for *yme1Δ* mutant in high glucose medium (Fig. 4B, left panel).

Another relevant parameter related to respiratory metabolism is the maintenance of the mitochondrial

membrane potential ( $\Delta\Psi$ ), which in turn is required for protein import into the mitochondria [26]. Using MitoTracker, a  $\Delta\Psi$ -dependent fluorescent dye, we detected a significant loss of  $\Delta\Psi$  in *yta12Δ* mutant and increased  $\Delta\Psi$  in *yme1Δ* cells, both results in consonance with our previous findings (Fig. 4C, Additional file 4: Fig. S1).

We presumed that the respiratory deficiency caused by the lack of the proteases Lon1 or Yta12 could be a consequence of impaired synthesis or assembly of the oxidative phosphorylation (OXPHOS) components encoded by the mitochondrial genome. To confirm this possibility, we isolated mitochondria from wild-type and deletion mutants and monitored the levels of several mitochondrial DNA (mtDNA)-encoded OXPHOS proteins by western blot. In *S. pombe*, seven subunits of the OXPHOS complexes are encoded by mtDNA, one belongs to complex III, three to complex IV, and three are part of the ATP synthase or complex V (Fig. 4D). Immunoblots in Fig. 4E show that the levels of Cox1, Cox2, Cox3, and Atp6 proteins are similar in wild-type and the long-lived mutants *mgr3Δ* and *yme1Δ*. However, the blots demonstrate highly reduced levels of these proteins in *lon1Δ* and *yta12Δ* mutants which might explain the respiratory defects observed in these strains.

To uncover the consequences of these alterations of the OXPHOS system, we measured H<sub>2</sub>O<sub>2</sub> abundance at the mitochondrial matrix by expressing the peroxide reporter HyPer7 at this subcellular compartment and determining its oxidation levels [27, 28]. The percentage of oxidation of this reporter depends on the steady-state H<sub>2</sub>O<sub>2</sub> levels at the matrix, being around 40% (OxD<sub>0</sub> of 0.4) in wild-type cells and increasing up to 60% when the main H<sub>2</sub>O<sub>2</sub> scavenger, Tpx1, is missing [28]. As shown in Fig. S2, the degree of oxidation of the probe in the long-lived mutants *mgr3Δ* and *yme1Δ* was undistinguishable from wild-type cells. In contrast, the *yta12Δ* strain displayed enhanced levels of basal probe oxidation (OxD<sub>0</sub> of 0.46) at the mitochondrial matrix compared to the wild-type strain (OxD<sub>0</sub> of 0.4), indicative of higher steady-state levels of H<sub>2</sub>O<sub>2</sub> (Additional file 5: Fig. S2). Cells lacking Lon1 displayed a slight increase in basal oxidation of MTS-Hyper7, suggesting that both short-lived mutants show enhanced production of mitochondrial ROS (Additional file 5: Fig. S2).

In summary, low respiratory capacity and enhanced ROS production correlate with a decrease in chronological lifespan whereas enhanced respiration might promote longevity.

### Mitochondrial dynamics as an important process modulating aging

Membrane fusion and fission are essential processes to preserve the distinctive morphology and number of healthy mitochondria. In fission yeast, mitochondrial fragmentation or fission is mediated by a dynamin-related GTPase Dnm1, which is recruited to the outer membrane (OM) by its receptor Fis1. Dnm1 forms a ring structure on the OM promoting membrane constriction and fission. Mitochondrial fusion instead is driven by the interaction of dynamin-like GTPases from opposing membranes [29]. In *S. pombe*, Fzo1 and Msp1 present in the OM and IM, respectively, are responsible for mitochondrial fusion (Fig. 5A).

To establish an association between mitochondrial dynamics and longevity, we first analyzed possible changes in mitochondrial morphology during chronological aging. We observed a severe mitochondrial fragmentation in wild-type aged cells grown in high glucose media (Fig. 5B). Additionally, fragmented mitochondria were accompanied by a reduction of  $\Delta\Psi$  measured using MitoTracker fluorescence (Additional file 6: Fig. S3). Similar events have been reported in budding yeast during replicative aging [14]. By contrast, mitochondrial fragmentation was only observed in aged cells of the fusion mutant *msp1Δ* and not in *dnm1Δ* and *fis1Δ* strains (Fig. 5B). In these two mutants, mitochondria were arranged like beads on a string (Fig. 5B), structures that may result from defective cristae formation [30].

Studies in model organisms have shown conflicting results about the impact of inhibiting mitochondrial fission on aging [17, 31]. Thus, both deletion and over-expression of the fission protein dynamin have been reported to increase lifespan. Monitoring cell survival

(See figure on next page.)

**Fig. 4** Short-lived strains, *lon1Δ* and *yta12Δ*, display dysfunctional mitochondria. **A** *lon1Δ* and *yta12Δ* exhibit a growth defect under low glucose conditions. 972 (WT), *lon1Δ*, *yta12Δ*, *mgr3Δ*, *yme1Δ*, and *cox6Δ* strains were grown in rich media (YE) with 3% glucose and minimal media (MM) with 2% glucose. Serial dilutions of logarithmically growing cells were spotted onto YE containing 3% or 0.08% glucose and MM containing 2% or 0.08% glucose plates. **B** Differences in oxygen consumption levels of mitoprotease mutants and *mgr3Δ*. The indicated strains were grown in rich media with 3% or 0.08% glucose. Oxygen consumption was measured when cultures reached an OD<sub>600</sub> of 0.5. Data from three biological replicates are shown. Significant differences between deletion strains and wild type were determined by two-sided *t*-test (\**p* < 0.05, \*\**p* < 0.01, \*\*\**p* < 0.001). **C** Mitochondrial membrane potential ( $\Delta\Psi$ ) is reduced in cells lacking the protease Yta12. Mitochondria of the indicated strains were stained with MitoTracker red and  $\Delta\Psi$  was determined by fluorescence microscopy. Maximum and minimum levels were adjusted using Fiji (ImageJ, National Institutes of Health) [65]. The corresponding quantification is shown in Fig. S1. Scale bar, 5  $\mu$ m. **D** Scheme depicting the localization of OXPHOS proteins encoded by mitochondrial DNA (mtDNA). **E** Short-lived strains have diminished steady-state levels of several mtDNA-encoded proteins. Mitochondrial TCA extracts of 972 (WT), *lon1Δ*, *yta12Δ*, *mgr3Δ*, and *yme1Δ* were analyzed by immunoblotting using antibodies against the mtDNA-encoded proteins Cox1, Cox2, Cox3, and Atp6. Sdh2-GFP was used as a loading control

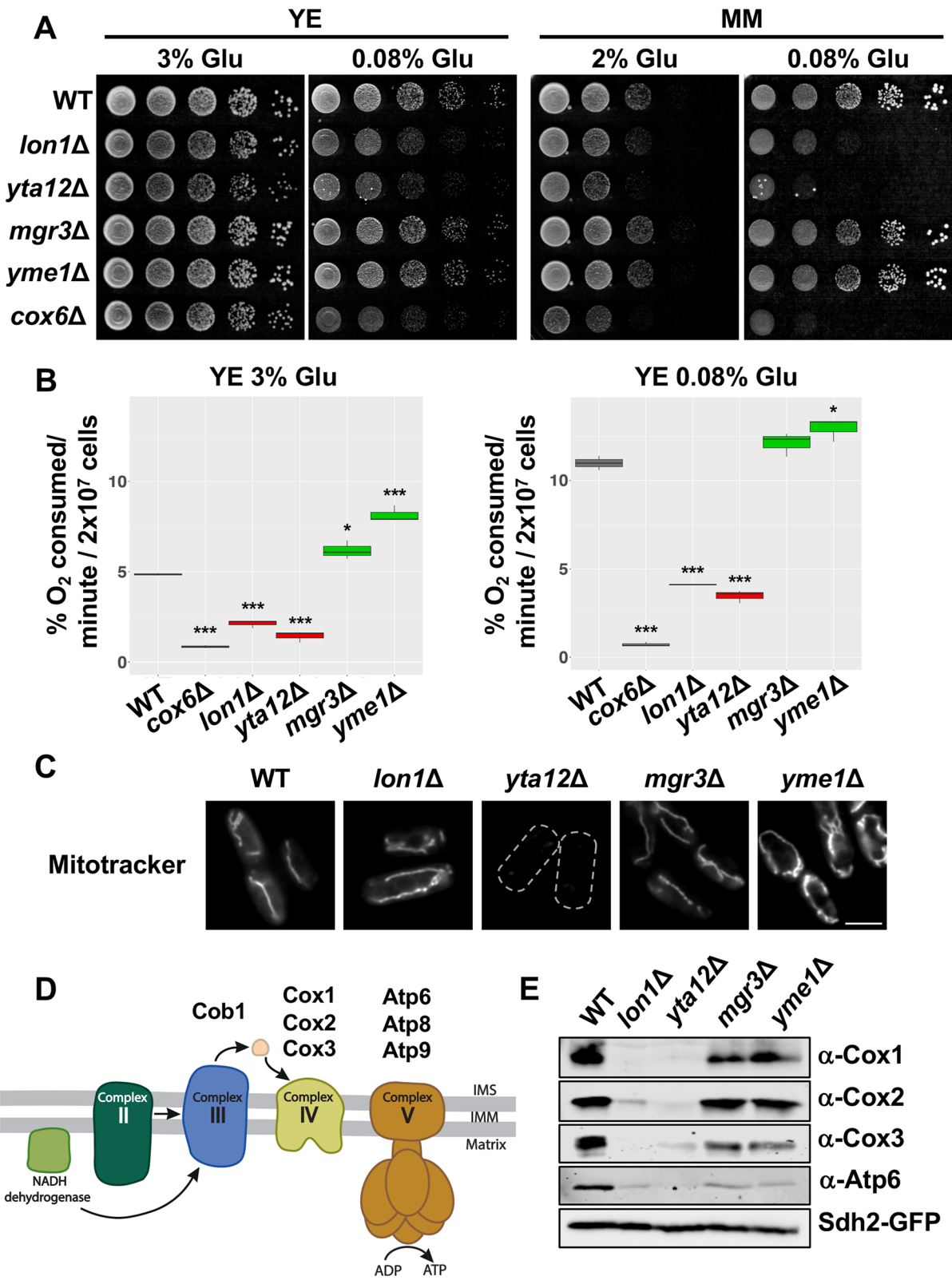


**Fig. 4** (See legend on previous page.)

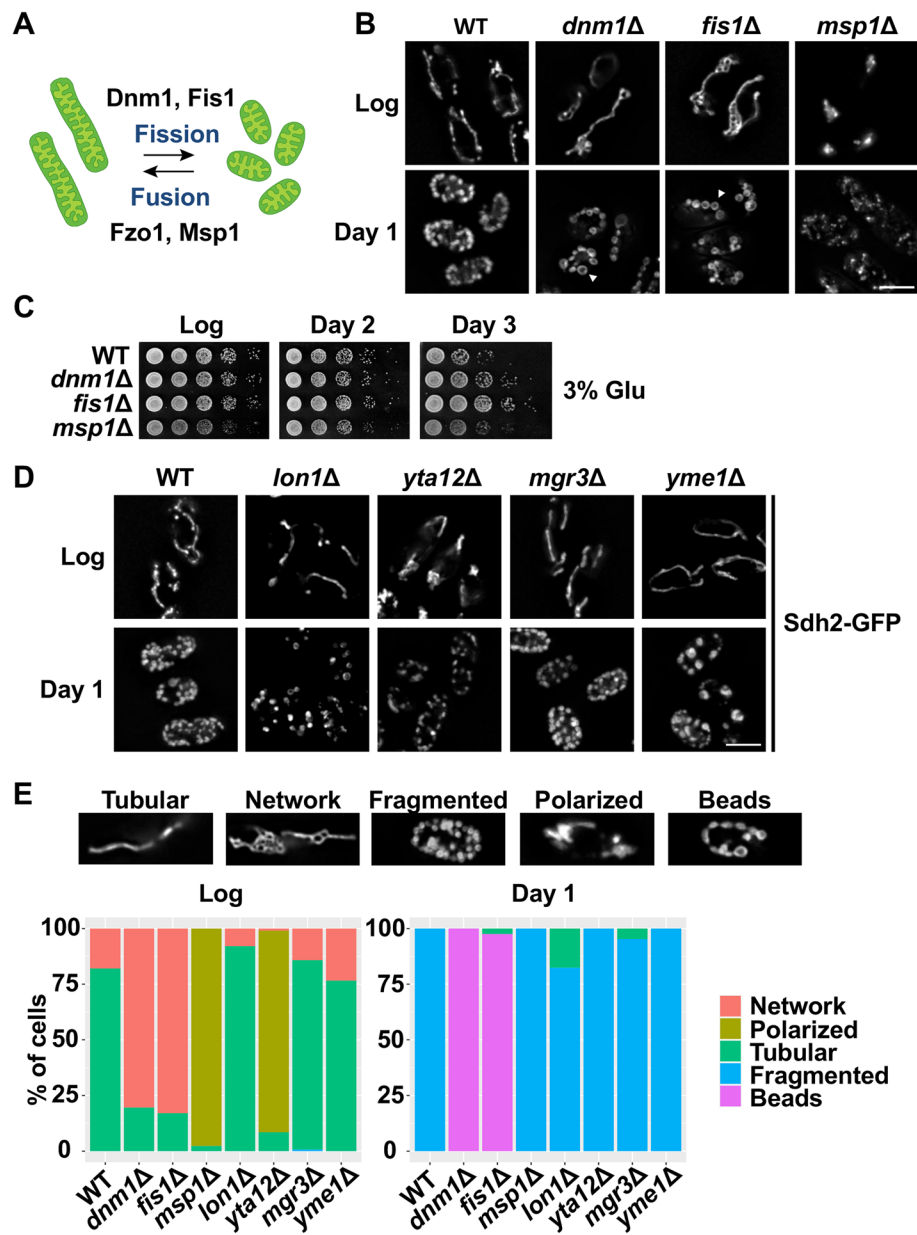


**Fig. 5** Influence of mitochondrial dynamics on chronological aging. **A** Scheme depicting the different proteins involved in mitochondrial fusion and fission. Dnm1 and Fis1 proteins mediate mitochondrial fission while Fzo1 and Msp1 are dedicated to mitochondrial fusion. **B** Mitochondrial morphology changes during chronological aging were determined by fluorescence microscopy in 972 (WT), *dnm1Δ*, *fis1Δ*, and *msp1Δ* strains expressing Sdh2-GFP. Cells were grown in rich media containing 3% glucose and analyzed after logarithmic growth (Log) and day 1 of the stationary phase. White arrows indicate mitochondria arranged like beads on a string. Scale bar, 5 μm. **C** *dnm1Δ* and *fis1Δ* strains show enhanced longevity. 972 (WT), *dnm1Δ*, *fis1Δ*, and *msp1Δ* cells were grown in rich media containing 3% glucose. Serial dilutions corresponding to culture samples from the logarithmic phase (Log) and days 2 and 3 of the stationary phase were spotted onto rich media plates. **D** Analysis of mitochondrial morphology in mitoprotease mutants and *mgr3Δ*. Fluorescence microscopy images of 972 (WT), *lon1Δ*, *yta12Δ*, *mgr3Δ*, and *yme1Δ* strains expressing the mitochondrial marker Sdh2-GFP. Cells were grown in rich media containing 3% glucose and analyzed after logarithmic growth (Log) and day 1 of the stationary phase. Scale bar, 5 μm. **E** Classification of mitochondrial morphology phenotypes. Mitochondria from 972 (WT), *dnm1Δ*, *fis1Δ*, *msp1Δ*, *lon1Δ*, *yta12Δ*, *mgr3Δ*, and *yme1Δ* were manually classified into five categories: tubular, network, fragmented, polarized, and beads. Images represent an example of each category. Bar plots show the percentage of cells from each category during logarithmic growth (Log) and day 1 of the stationary phase ( $n > 100$ )



during chronological aging, we have found that deletion of the fission genes *dnm1* or *fis1* caused a significant increase of longevity whereas the loss of the fusion GTPase *Msp1* had no effect on lifespan (Fig. 5C). This result is consistent with the increased RLS observed upon deletion of *Dnm1* or *Fis1* in budding yeast [17].

Considering these results, we hypothesized whether the longevity phenotype of the mitoprotease mutants could be explained by any alteration in their fusion-fission equilibrium. We used an image analysis tool (MiNA) [32] to measure the length and branches of mitochondrial structures in logarithmically growing cells. While the fusion and fission mutants displayed decreased and enhanced elongation capacities, respectively, the protease mutants *lon1Δ*, *mgr3Δ*, and *yme1Δ* did not differ from the control, dismissing a straightforward correlation between longevity and mitochondrial fusion/fission (Fig. 5D, Additional file 7: S4). To better characterize possible changes in mitochondrial morphology triggered by aging, we sorted the observed structures into five classes: network, polarized, tubular, fragmented, and beads (Fig. 5E). After logarithmic growth, wild-type, *lon1Δ*, *mgr3Δ*, and *yme1Δ* strains showed tubular mitochondria, whereas mitochondria in *dnm1Δ* and *fis1Δ* mutants were distributed as a branched network (Fig. 5D, E). Interestingly, the short-lived mutant *yta12Δ* displayed aggregated mitochondria at the cell poles similar to *mcp1Δ* cells, suggesting that this matrix protease may participate in the regulation of mitochondrial fusion (Fig. 5D, E). Upon chronological aging, all mitochondrial protease mutants exhibited fragmented mitochondria as described earlier for wild-type cells (Fig. 5D, E). Thus, we conclude that the longevity phenotypes of our mitochondrial protease mutants cannot be explained by their mitochondrial fusion and fission properties.

### During chronological aging, mitophagy contributes to lifespan extension

Several studies demonstrate the anti-aging role of mitophagy facilitating the removal of dysfunctional or damaged mitochondria [33–35]. To uncover the relevance of mitophagy during chronological aging, we first analyzed mitophagy induction in cells grown for different time points in rich (3% Glu) and low glucose (1% Glu) media (Fig. 6A). Mitophagy was monitored here by the cleavage of the mitochondrial protein Sdh2-GFP and the release of GFP which occurs during mitochondria degradation by autophagy [21]. Using this assay, we only detected mitophagy activation in low glucose conditions that promote respiratory growth and hence the turnover of mitochondria (Fig. 6A). Moreover, the degradation of Sdh2-GFP observed under low glucose conditions was inhibited in the autophagy mutant *atg8Δ*, demonstrating unequivocally that this process is autophagy-dependent (Fig. 6B). In agreement with these results, Sdh2-GFP only colocalized with a vacuole marker (Cpy1-mCherry) in aged cells after growth in a low glucose medium (Fig. 6C).

Recently, the mitophagy receptor Atg43 has been identified in fission yeast allowing the study of the specific role of mitophagy in lifespan extension [23]. To this end, we examined first whether Atg43 is required for mitophagy during chronological aging. Using low glucose conditions and *atg43-1* mutant with a partial deletion of the gene, we observed a complete inhibition of the mitophagy process (Fig. 6D), resembling the effect reported under nitrogen starvation [23]. In the next step, we assayed the lifespan of the *atg43-1* mutant in low glucose conditions and found a decrease in longevity compared to the wild-type strain (Fig. 6E, Additional file 8: S5A), supporting the need of active mitophagy to prevent premature aging.

(See figure on next page.)

**Fig. 6** Impact of mitophagy inhibition on chronological lifespan. **A** Mitophagy is induced during the stationary phase in low glucose conditions. Mitophagy was monitored by the cleavage of Sdh2-GFP detected by immunoblotting with an anti-GFP antibody. A wild-type strain (972) was grown in rich media containing 3% glucose (3% Glu) or 1% glucose (1% Glu). Samples correspond to TCA extracts of cell cultures after logarithmic growth (day 0) and days 1, 2, and 3 of the stationary state. Sty1 levels were used as a loading control. **B** Deletion of *Atg8* inhibits processing of Sdh2-GFP during the stationary phase. Mitophagy induction in 972 (WT) and *atg8Δ* strains was monitored by immunoblotting as in **A**. Samples correspond to TCA extracts from logarithmic growth (day 0) and days 1, 2, and 3 of the stationary state. Sty1 levels were used as a loading control. **C** Colocalization of the mitochondrial marker Sdh2-GFP and the vacuolar marker Cpy1-mCherry. Wild-type cells grown in rich media with 3% glucose (3% Glu) or 1% glucose (1% Glu) were visualized during logarithmic growth (Log) and day 3 of the stationary phase. Insets show a magnified region containing vacuoles labeled with GFP and Cpy1-mCherry. Scale bar, 5 μm. **D** *atg43-1* mutant blocks mitophagy during the stationary phase at low glucose conditions. Mitophagy in 972 (WT) and *atg43-1* strains was monitored by the cleavage of Sdh2-GFP detected by immunoblotting with an anti-GFP antibody. Samples correspond to TCA extracts of cell cultures grown in media with 1% glucose and collected after logarithmic growth (day 0) and days 1, 2, and 3 of the stationary state. Ponceau was used as the loading control. Bar plot represents the mean and SD of the GFP/Sdh2-GFP ratio from three independent experiments. Quantification was performed using Image Lab software. Significant differences between the *atg43-1* strain and wild type were determined by a two-sided *t*-test ( $***p < 0.001$ ). **E** Inhibition of mitophagy reduces cell longevity under low glucose conditions (1% Glu). Lifespan of 972 (WT), *pka1Δ*, *sty1Δ*, and *atg43-1* strains was measured by propidium iodide staining and FACS. Line plot represents the local regression curves for the average survival of each strain ( $n > 10$ ) at different time points. Each survival curve also displays a 95% confidence interval band. Bar plot depicts the average area under the curve of each strain, and error bars represent SD. Significant differences between deletion strains and wild type were determined by a two-sided *t*-test ( $*p < 0.05$ ,  $**p < 0.01$ ,  $***p < 0.001$ )

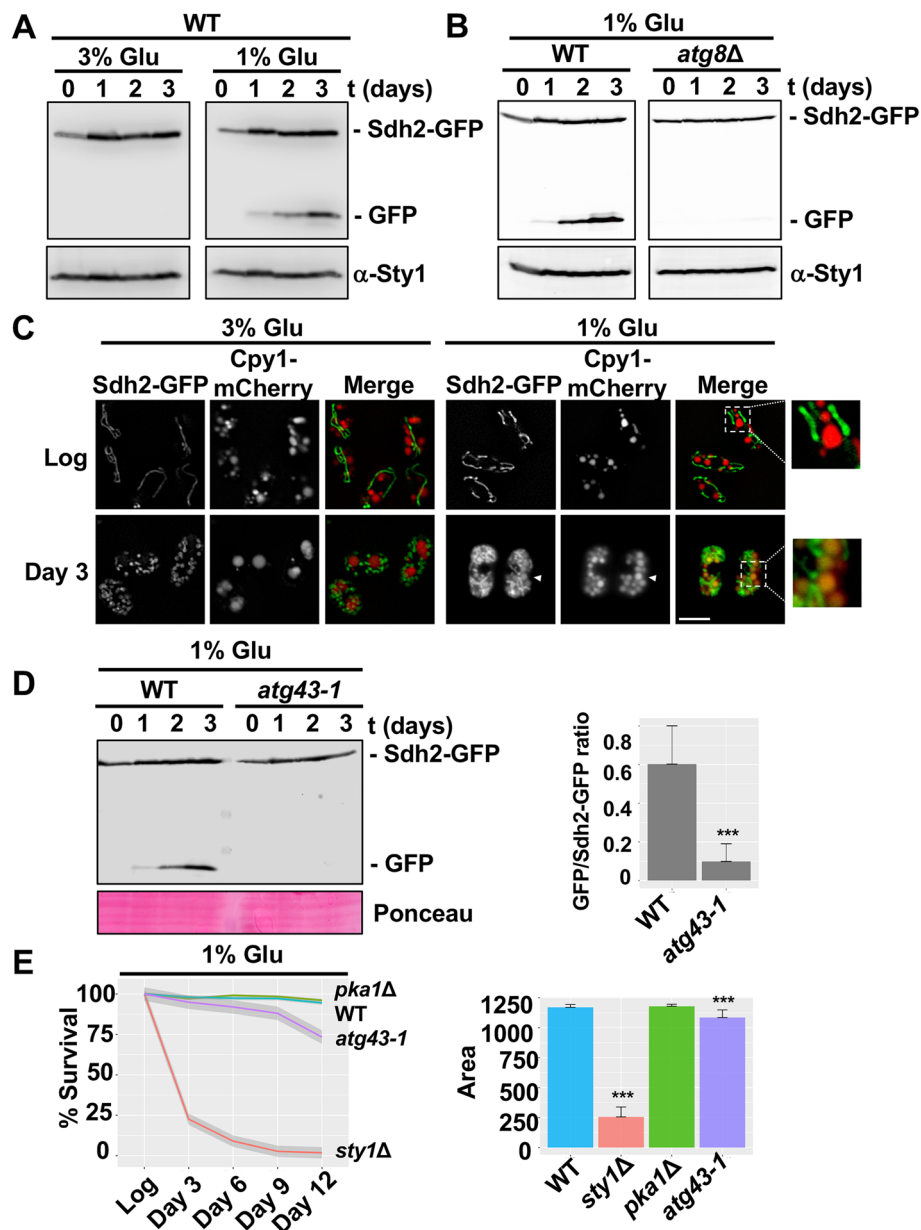


**Fig. 6** (See legend on previous page.)

Similar results were obtained in budding yeast using the mutant lacking the mitophagy receptor Atg32, but under severe caloric restriction conditions [35].

In *S. pombe*, three Atg proteins, Atg20, Atg24, and Atg24b, have also been implicated in the degradation of mitochondria by autophagy [22]. Comparable to the *atg43-1* mutant (Fig. 6D, E), double deletion of these Atg proteins led to impaired mitophagy (Additional file 8: Fig. S5B) and decreased survival (Additional file 8: Fig. S5C) during chronological aging after growth in low glucose media.

We questioned whether mitophagy activation could mediate lifespan extension in the long-lived mutants *mgr3Δ* and *yme1Δ*. To test this possibility, we analyzed Sdh2-GFP processing in the mitoprotease deletion mutants and *mgr3Δ* after growth in high and low glucose media. *mgr3Δ* and *yme1Δ* mutants with increased longevity displayed enhanced mitophagy induction compared to wild-type strain, specially *mgr3Δ* cells, where mitophagy was stimulated even in rich media (Fig. 7A, Additional file 9: Fig. S6A). By contrast, mitophagy induction during chronological aging was not detected in

the short-lived strains *lon1Δ* and *yta12Δ* (Fig. 7A, Additional file 9: Fig. S6A). These results point to a potential association between mitophagy activation and increased lifespan.

To confirm if mitophagy contributes to the increase in longevity observed in *mgr3Δ* and *yme1Δ*, we analyzed the CLS of the double mutants grown in high glucose media. Defective Atg43 and in turn impaired degradation of mitochondria reduced the longevity of both mutants to wild-type levels indicating that mitophagy induction is critical for the lifespan extension of *mgr3Δ* and *yme1Δ* cells (Fig. 7B). Interestingly, *atg43-1* did not reduce the lifespan in a wild-type background and high glucose media (Fig. 7B), supporting the idea that mitophagy is required to sustain improved longevity in a context of increased respiration, such as wild-type cells under calorie restriction (Fig. 6E) [35] and long-lived deletion mutants under glucose-rich conditions (Fig. 7B). In contrast, mitophagy inhibition by *atg43-1* had no negative effect on the lifespan of the short-lived mutants *lon1Δ* and *yta12Δ* (Additional file 9: Fig. S6B). Considering our findings, we can conclude that functional mitophagy represents a common anti-aging strategy shared by worms, flies, and yeast models.

## Discussion

Using a genome-wide screening, we have identified almost 500 deletion mutants of fission yeast with altered lifespan, among them four mutants associated with protein maturation/degradation at the mitochondria. The analysis of different mitochondrial processes in these mutants revealed that increased respiration can mediate a significant extension of chronological lifespan when it is combined with enhanced mitophagy (Fig. 7B, C). Both processes guarantee cell survival during chronological aging; a high respiratory activity ensures an efficient energy production whereas mitophagy is required to maintain a functional pool of mitochondria. Our results also support that the positive effect of respiration on longevity is achieved during logarithmic growth; during this

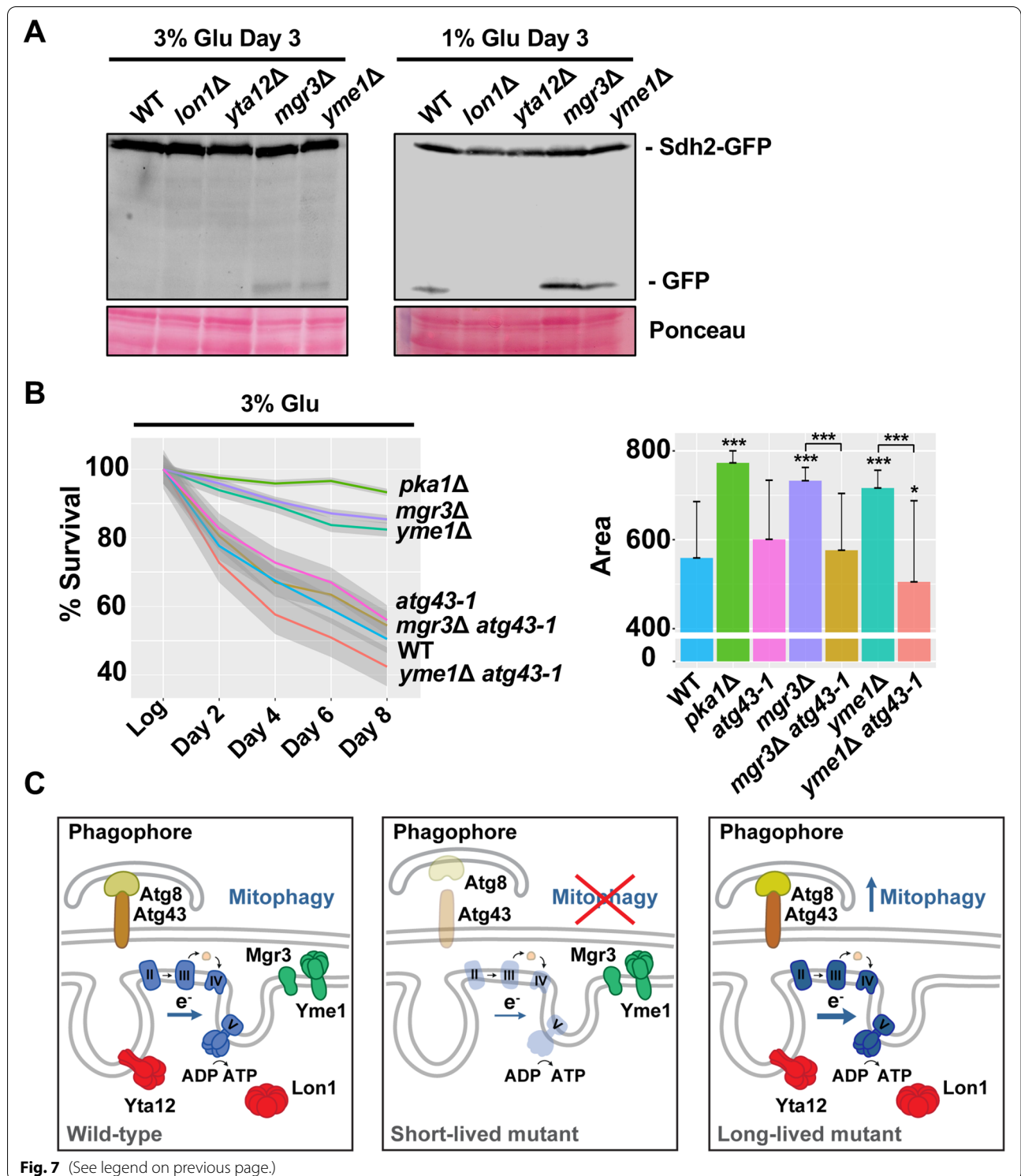
period of adaptation, cells become prepared to survive in more adverse conditions. On the other hand, low respiratory metabolism caused by OXPHOS-deficient mitochondria, and mitophagy inhibition are associated with premature chronological aging. Moreover, we uncovered possible connections of the mitochondrial PQC, and in particular the activity of some mitoproteases and the adaptor protein Mgr3 with the synthesis of mtDNA-encoded ETC components, the induction of mitophagy, and the regulation of mitochondrial fusion/fission events.

In our screening, *lon1Δ* and *yta12Δ* have been characterized as short-lived mutants. Both deletion strains showed poor growth in respiratory media and reduced oxygen consumption (Fig. 4A, B). This respiratory deficiency could be explained at least partially by a decrease in the levels of OXPHOS components (Fig. 4E). Studies in budding yeast have previously linked deletion of OXPHOS subunits or inhibition of complex III with reduced respiration and decreased CLS [36, 37]. Likewise, deletion of ETC subunits or impaired assembly of OXPHOS complexes shortens RLS [38]. Interestingly, deletion or inhibition of ETC components might also cause increased lifespan. This effect has been associated with reduced ROS production in yeast or activation of stress responses in *C. elegans* and mice (UPR<sup>mt</sup>, the transcription factors HSF-1 or HIF1 pathways) [39–42].

Lon1 protease mediates the degradation of misfolded or damaged proteins in the mitochondrial matrix [43–45]. In agreement with our results, it has been shown that deletion of the budding yeast homolog Pim1 results in accelerated aging [46] whereas LON protease overexpression leads to increased healthspan in the fungus *P. anserina* [47]. In fission yeast, one of the Lon1 substrates identified is Ppr10 which functions as mitochondrial translation activator [48]. We speculate that the low levels of some OXPHOS components observed in *lon1Δ* mutant might be caused by the loss of Ppr10 degradation and in turn defective control of mitochondrial translation. Additionally, the function of Lon protease has been linked with mtDNA stability and transcription,

(See figure on next page.)

**Fig. 7** Mitophagy is required for lifespan extension in the long-lived mutants *mgr3Δ* and *yme1Δ*. **A** Monitoring mitophagy induction in *lon1Δ*, *yta12Δ*, *mgr3Δ*, and *yme1Δ* strains. The experiment was performed as in Fig. 6A. Samples correspond to cells grown in rich media containing 3% or 1% glucose and day 3 of the stationary phase. Ponceau was used as the loading control. Quantification of mitophagy activation is shown in Fig. S6A. **B** Mitophagy contributes to the longevity extension observed in *mgr3Δ* and *yme1Δ* strains under high glucose conditions (3% Glu). Lifespan of 972 (WT), *pka1Δ*, *mgr3Δ*, *yme1Δ*, *atg43-1*, *mgr3Δ atg43-1*, and *yme1Δ atg43-1* strains was measured by propidium iodide staining and FACS. Line plot represents the local regression curves for the average survival of each strain ( $n > 10$ ) at different time points. Each survival curve also displays a 95% confidence interval band. Bar plot depicts the average area under the curve of each strain, and error bars represent SD. Significant differences between deletion strains and wild type, and *mgr3Δ* and *yme1Δ* mutants versus *mgr3Δ atg43-1* and *yme1Δ atg43-1*, respectively, were determined by a two-sided *t*-test (\* $p < 0.05$ , \*\* $p < 0.01$ , \*\*\* $p < 0.001$ ). **C** Model depicting the effect of deletion of the three mitochondrial proteases and the adaptor protein Mgr3 on longevity. Short-lived mutants, *lon1Δ* and *yta12Δ*, are characterized by impaired respiration and loss of mitophagy which curtail cell survival during the stationary phase. Conversely, in long-lived mutants, *mgr3Δ* and *yme1Δ*, enhanced respiratory activity together with the elimination of damaged mitochondria by mitophagy contribute to the extension of chronological lifespan



which could explain the reduced content of certain OXPHOS proteins in this mutant [49]. In budding yeast, the absence of OXPHOS subunits in *yta12Δ* mutant has been connected with impaired maturation of its

substrate MrpL32, a mitochondrial ribosome subunit [50]. Despite the similar deficiency in OXPHOS components, *yta12Δ* cells showed higher levels of H<sub>2</sub>O<sub>2</sub> compared to *lon1Δ* mutant (Additional file 5: Fig. S2). This

finding is consistent with the different gene expression signatures reported for these two mutants, with *yta12Δ* cells exhibiting a potent induction of the genes involved in the stress response [51].

Our CLS screening has also revealed two long-lived mutants *mgr3Δ* and *yme1Δ* with enhanced oxygen consumption specially in high glucose conditions (Fig. 4B). Multiple studies support a link between increased respiration and lifespan extension [5, 52, 53]. A higher respiration rate has also been detected in long-lived strains of wild yeast isolates [54]. This effect is often a consequence of the activation of stress responses which promote defense mechanisms and/or mitochondrial biogenesis. Similarly, in budding yeast, increased CLS in cells lacking the sirtuin Sir2 has been connected to high respiratory capacity and resistance to different stressors [36, 55–58]. Lifespan extension in *mgr3Δ* and *yme1Δ* mutants seems to be independent of altered ROS levels at the matrix (Additional file 5: Fig. S2), but further work is required to exclude a contribution of stress pathways in these mutants. An additional explanation for the long-lived phenotype of *mgr3Δ* and *yme1Δ* cells could be a higher content of trehalose, an essential storage carbohydrate which has been linked with increased survival during the stationary phase [36].

Another aspect of mitochondrial homeostasis to consider is the degradation of damaged mitochondria by mitophagy. Indeed, impaired mitophagy causes reduced CLS in yeast and accelerated aging in human cells [35, 59]. In contrast, activation of mitophagy might contribute to lifespan extension [33, 34]. For instance, in yeast cells, expression of human Parkin, an E3 ubiquitin ligase required for mitophagy, prolongs CLS under respiratory conditions likely via activation of mitophagy [60]. Our analysis of the protease deletion mutants demonstrates an unambiguous correlation between lifespan and mitophagy: in the short-lived mutants *lon1Δ* and *yta12Δ*, we did not detect signs of mitophagy, while the process was enhanced in the long-lived mutants *mgr3Δ* and *yme1Δ* (Fig. 7A, Additional file 9: Fig. S6A). Moreover, mitophagy inhibition caused by *atg43-1* mutant restored wild-type lifespan in both long-lived mutants, supporting the notion that mitophagy is essential for their long lifespan phenotype (Fig. 7B). In budding yeast, Yme1 has also been linked to mitophagy regulation, but its deletion has the opposite phenotype; this protease is required for the processing of the receptor protein Atg32 and therefore essential for mitophagy [61].

During the characterization of the mitochondrial PQC mutants, we could not prove a direct link between longevity and mitochondrial morphology (Fig. 5E). However, we have identified Yta12 as a regulator of mitochondrial fusion, and future studies will reveal the molecular

events driven by this protease regarding mitochondrial morphology. Based on the analysis of respiration and mitophagy, we can conclude that these processes are intimately interconnected (Figs. 4 and 6). Short-lived mutants *lon1Δ* and *yta12Δ* were defective in respiration and mitophagy whereas both activities were stimulated in the long-lived mutants *mgr3Δ* and *yme1Δ*. In order to extend lifespan, a high respiratory activity should be accompanied by efficient elimination of damaged mitochondria and the decline of both activities results in severe lifespan shortening. The signaling cascades connecting these two processes, enhanced respiratory activity and mitophagy, are still to be determined.

## Conclusions

In this study, we developed a genome-wide knockout screen searching for fission yeast mutants with altered longevity. Thanks to this approach and the following analysis, we identified four deletion mutants acting at the mitochondria that are implicated in protein quality control. These four mutants exhibited opposite longevity phenotype; while the lack of the proteases Lon1 or Yta12 shortened lifespan, the absence of the protease Yme1 or its adaptor protein Mgr3 caused increased lifespan. Additionally, we demonstrate that mitophagy is required for lifespan extension in wild-type cells upon glucose depletion and in the long-lived mutants *mgr3Δ* and *yme1Δ* under glucose-rich conditions. Hence, this work provides important insights into the modulation of cell longevity by respiration and mitophagy.

## Methods

### Yeast strains

Yeast strains were grown in rich medium (YE) or minimal medium (MM) with the indicated glucose concentrations at 30 °C as previously described [62]. Genotypes of strains used are described in Additional file 11: Table S4.

### Strains and growth conditions for chronological lifespan screening

To perform the chronological aging screening, we used the deletion mutant library of Bioneer version 2.0 which contains 3004 strains. First, the frozen stock of the deletion collection strains was plated into YE plates and incubated at 30 °C. After 2 days, cells were inoculated in 96-well plates containing 150 μl of YE with 3% glucose media. The following day, 10 μl of these cells was transferred into 500 μl of YE with 3% glucose media in 1.3-ml 96-well plates that were incubated at 30 °C with constant agitation. After an overnight incubation (considered logarithmic growth), we started measuring cell viability taking samples every 2 days (days 2, 4, 6, and 8) of stationary growth. Cell viability was measured using



propidium iodide (PI) [24]. A total of 10  $\mu\text{l}$  of cultured cells was incubated in 200  $\mu\text{l}$  of PBS with 2  $\mu\text{M}$  of PI during 30 min at 30 °C in the dark. Ten thousand cells were analyzed by flow cytometry, using BD FACSCanto™, and PI staining was monitored using PE-A, which detects red fluorescence. We extracted the data of percentage of living cells to build survival curves, considering that the Log sample is 100% of viable cells. Strains that presented no growth or regrowth after several days in the stationary phase were not included in the analysis. 666 (WT), *sty1* $\Delta$ , and *pka1* $\Delta$  were included as average, short-lived, and long-lived control strains, respectively. Control strains were included in each of the 96-well plates analyzed.

#### Statistical analysis of chronological lifespan screening

The area under the survival curve was calculated as in [63], and it was selected as the parameter to compare the longevity among the strains. Three longevity distributions were defined based on the control strains: average, short-, and long-lived survival. Employing a Bayesian inference model, an equal prior probability for each mutant to belong to each distribution was first established. These priors were then reallocated based on deletion strain survival results, using a Student's *t*-test. The resulting posterior probabilities were then used to assign each mutant to the model with the highest probability.

#### GO enrichment analysis

GO enrichment in Cellular Component and Biological Process was obtained using Metascape [64] from a single list that contains the short-lived (163) and long-lived (309) strains. The parameters used were 3 (minimum overlap), 0.05 (*P*-value cutoff), and 1.5 (minimum enrichment).

#### Spot assay

Cells were grown in YE or MM at 30 °C until the stationary phase was reached. The same concentration of cells ( $\text{OD}_{600}$  2.5) and 1/10 serial dilutions of culture samples corresponding to logarithmic growth ( $\text{OD}_{600}$  0.5) and different days of stationary phase were spotted onto YE or MM plates with the indicated glucose concentration. The spots were allowed to dry, and the plates were incubated at 30 °C for 2–4 days.

#### In vivo measurement of matrix $\text{H}_2\text{O}_2$ levels using MTS-HyPer7

A detailed description of plasmid construction and the experimental procedure has been published [28]. Briefly, plasmid p730 carrying the reporter HyPer7 with the MTS (mitochondrial targeting sequence) of Aco1 was transformed in the mitochondrial protease mutants. HyPer7 has two excitation maxima at 400 and 499 nm and one

emission peak at 516 nm [27]. We used excitation filters of 400–10 and 485BP12, combined with an emission filter of EM520 in a FLUOstar OMEGA (BMG Labtech). For the experiments shown here, MM-based early stationary phase pre-cultures were diluted in filtered MM to reach an  $\text{OD}_{600}$  of 1 after 4–5 duplications. The fluorescence of 190  $\mu\text{l}$  of these cultures was directly monitored in 96-well plates (Krystal Microplate™ 215,003, Porvair Sciences). The two excitation wavelengths were recorded, and after 4 cycles of approximately 2 min each, 10  $\mu\text{l}$  of the indicated  $\text{H}_2\text{O}_2$  treatments were added to accomplish the final concentrations of  $\text{H}_2\text{O}_2$ . In two wells, final concentrations of 50 mM dithiothreitol (DTT) and 1 mM of  $\text{H}_2\text{O}_2$  were added as controls of fully reduced and oxidized reporter, respectively. A formula described in [28] was applied to determine the degree of oxidation of the  $\text{H}_2\text{O}_2$  sensor MTS-HyPer7. For each strain, we grew cultures of the wild-type background 972 and performed the same treatments on 96-well plates; after recording, we subtracted the fluorescence values of the wild-type strain to those of the strain expressing the reporter. Graphics represent the mean of three independent experiments.

#### Microscopy and image analysis

Samples from cell cultures in the logarithmic phase and after reaching the stationary phase grown in YE with 3% or 1% glucose were harvested by centrifugation and visualized at room temperature. Images were acquired using a Nikon Eclipse 90i microscope equipped with differential interference contrast optics, a PLAN APO VC 100 $\times$ 1.4 oil immersion objective, an ORCA-II-ERG camera (Hamamatsu), excitation and emission filters GFP-4050B, mCherry-C (Semrock), and image acquisition software Metamorph 7.8.13 (Gataca Systems). Processing of all images was performed using Fiji (ImageJ, National Institutes of Health) [65]. Mitochondria network morphology analysis was conducted with the algorithm MiNa [32]. To compare mitochondria of different strains, we chose the parameter summed branch length mean, which represents the mean of the sum of the lengths of branches for each independent structure. To cover a larger volume of the cell, z-stacks of 9 images with 0.3- $\mu\text{m}$  spacing were acquired, deconvolved, and represented in single images as maximum-intensity projections. At least 50 cells from each strain were analyzed. For Mitotracker staining, cell cultures at  $\text{OD}_{600}$  0.5 were incubated with 0.1  $\mu\text{g}/\text{ml}$  MitoTracker Red CMXRos (Invitrogen) during 30 min. Cells were washed, centrifuged, and resuspended in YE with 3% glucose. For quantification of  $\Delta\Psi$ , the integrity density was measured after segmentation of bright-field images. The Fiji-based macro for image segmentation was designed by Sébastien Tosi (Institute for Research

in Biomedicine, Barcelona). At least 100 cells from each strain were analyzed.

### TCA extracts and immunoblot analysis

Modified trichloroacetic acid (TCA) protein extracts were prepared as previously described [66]. Proteins were separated by SDS-PAGE and detected by immunoblotting with monoclonal anti-GFP (Takara). Anti-Sty1 polyclonal antibody [67] was used in the loading control. Antibodies used to detect mitochondrial encoded proteins Cox1, Cox2, Cox3, and Atp6 were described in [48]. StartBright Blue 700 Fluorescence anti-Mouse secondary antibody (Bio-Rad) was used for quantification of mitophagy induction.

### Mitochondria purification

Mitochondria were purified from protoplasts prepared using the Zymolyase and lysing enzymes from *Trichoderma harzianum* as described in [68]. Briefly, protoplasts were broken by 10 strokes using a glass homogenizer, and mitochondria-enriched fraction was obtained after two centrifugation steps at 800 g and 12000 g. For western blot analysis, proteins were precipitated with 10% TCA as described above.

### Oxygen consumption

Oxygen consumption was performed as described previously [10]. Cells were harvested and  $2 \times 10^7$  cells resuspended in 1 ml of MM to a final OD<sub>600</sub> of 1. The measurements were made using a Hansatech Oxygraph (Hansatech), with readings being recorded during 10 min. Each one of the measurements was performed from biological triplicates.

### Quantification and statistical analysis

Quantification of western blots was performed using Image Lab software (Bio-Rad). Unless otherwise stated, all experiments were performed at least three times and representative experiments were shown.

### Abbreviations

AAA: ATPases associated with diverse cellular activities; ATG: Autophagy-related; CLS: Chronological lifespan; GFP: Green fluorescent protein; Glu: Glucose; GO: Geneontology; ETC: Electron transport chain; i-AAA: Mitochondrial inner membrane ATPases associated with diverse cellular activities; IM: Mitochondrial inner membrane; IMS: Mitochondrial intermembrane space; Log: Logarithmic growth; Lon1: Lon peptidase 1; m-AAA: Mitochondrial matrix ATPases associated with diverse cellular activities; Mgr3: Mitochondrial genome required 3; MM: Minimal medium; mtDNA: Mitochondrial DNA; MTS: Mitochondrial targeting sequence; OD: Optical density; OM: Mitochondrial outer membrane; OXPHOS: Oxidative phosphorylation; PI: Propidium iodide; PQC: Protein quality control; RLS: Replicative lifespan; ROS: Reactive oxygen species; *S. cerevisiae*: *Saccharomyces cerevisiae*; *S. pombe*: *Schizosaccharomyces pombe*; TCA: Trichloroacetic acid; UPRmt: Mitochondrial unfolded protein response; WT: Wild-type; YE: Yeast extract; Yme1: Yeast mitochondrial escape 1; Yta12: Yeast Tat-binding Analog 12;  $\Delta\Psi$ : Mitochondrial membrane potential.

## Supplementary Information

The online version contains supplementary material available at <https://doi.org/10.1186/s12915-022-01352-w>.

**Additional file 1: Table S1.** Deletions strains analyzed in this study.

**Additional file 2: Table S2.** Short and long-lived mutants identified in this study.

**Additional file 3: Table S3.** Gene Ontology enrichment analysis.

**Additional file 4: Fig. S1.** Deletion of the protease Yta12 results in decreased mitochondrial membrane potential. Quantification of the mitochondrial membrane potential ( $\Delta\Psi$ ) of 972 (WT), *lon1Δ*, *yta12Δ*, *mgr3Δ* and *yme1Δ* cells stained with Mitotracker Red. Violin plot represents the integrated density from at least 100 cells of each strain. Significant differences between deletion strains and wild type were determined by two-sided *t*-test (\*  $p < 0.05$ , \*\*  $p < 0.01$ , \*\*\*  $p < 0.001$ ). Right panel shows an example of the segmentation of bright-field (BF) images performed using a Fiji-based macro.

**Additional file 5: Fig. S2.** Analysis of ROS levels in mitochondrial protease mutants. A Levels of H<sub>2</sub>O<sub>2</sub> in the mitochondrial matrix were determined in 972 (WT), *lon1Δ* and *yta12Δ*, *mgr3Δ* and *yme1Δ* strains expressing the reporter MTS-HyPer7. The indicated concentrations of H<sub>2</sub>O<sub>2</sub> or DTT were directly added to cultures grown in MM and 96-well imaging plates. Fluorescence was monitored at 30°C for the indicated time points. The degree of probe oxidation (amount of probe oxidized per 1) is shown in the Y-axis (OxD); the starting level of probe oxidation (OxD<sub>0</sub>) for wild-type and *yta12Δ* strains is indicated with dashed lines. For each strain, average data from three biological replicates are shown. B Basal level of probe oxidation (OxD<sub>0</sub>) from Figure S2A strains. Each bar represents mean and SEM from four biological replicates. Significant differences between deletion strains and wild type were determined by two-sided *t*-test (\*  $p < 0.05$ , \*\*  $p < 0.01$ , \*\*\*  $p < 0.001$ ).

**Additional file 6: Fig. S3.** Changes in mitochondrial function and morphology during chronological aging. Fluorescence microscopy of wild-type cells expressing the mitochondrial marker Sdh2-GFP and stained with MitoTracker red to measure membrane potential. Cells were grown in rich media containing 3% glucose and analyzed during logarithmic growth (Log) and stationary phase (days 1, 2 and 3). Maximum and minimum levels were adjusted using Fiji software. Scale bar, 5 μm.

**Additional file 7: Fig. S4.** Quantification of mitochondrial lengths during logarithmic growth. Mitochondrial length of 972 (WT), *dnm1Δ*, *fts1Δ*, *msp1Δ*, *lon1Δ*, *yta12Δ*, *mgr3Δ* and *yme1Δ* strains was determined using the parameter "Summed branch lengths mean" of the MiNa software [32] ( $n > 50$ ). Significant differences between deletion strains and wild type were determined by two-sided *t*-test (\*  $p < 0.05$ , \*\*  $p < 0.01$ , \*\*\*  $p < 0.001$ ). Fluorescence microscopy images represent an example of the process of binarization and skeletonization done using MiNa software.

**Additional file 8: Fig. S5.** Monitoring mitophagy induction and chronological lifespan in autophagy mutants. A Inhibition of mitophagy reduces cell longevity under low glucose conditions (1% Glu). Serial dilutions of 972 (WT) and *atg43-1* strains growing in media with 1% glucose were spotted after logarithmic growth (Log) and days 3, 5 and 9 of stationary state. B Fluorescence microscopy of ZD307 (WT), *atg5Δ*, *atg20Δ*, *atg24Δ*, *atg24Δ atg24bΔ* and *atg20Δ atg24Δ atg24bΔ* strains expressing the mitochondrial marker Sdh2-mCherry. Cells were grown in rich media containing 3% or 1% glucose and analyzed after logarithmic growth (Log) and day 3 of stationary phase. Images represent maximum-intensity projections of deconvolved z stacks (9 planes, 0.3 μm steps). White arrows indicate vacuoles labeled with mCherry signal. Scale bar, 5 μm. C Cells lacking the Atg proteins involved in organelle-autophagy exhibit a reduced lifespan. ZD307 (WT), *atg20Δ atg24Δ*, *atg24Δ atg24bΔ* and *atg20Δ atg24Δ atg24bΔ* strains were grown in rich media with 1% glucose. Serial dilutions corresponding to culture samples from logarithmic phase (Log) and days 3, 5 and 7 of stationary phase were spotted onto rich media plates.

**Additional file 9: Fig. S6.** Mitophagy inhibition in the short-lived strains *lon1Δ* and *yta12Δ*. A Quantification of mitophagy induction using Image lab software. Bar plots represent mean and SD of GFP/Sdh2-GFP ratio

from three independent experiments. Significant differences between deletion strains and wild type were determined by two-sided *t*-test (\*  $p < 0.05$ , \*\*  $p < 0.01$ , \*\*\*  $p < 0.001$ ). B *atg43-1* mutant does not reduce further the lifespan of the short-lived mutants *lon1Δ* and *yta12Δ*. Lifespan of 972 (WT), *sty1Δ*, *atg43-1*, *lon1Δ*, *lon1Δ yta12Δ*, and *yta12Δ atg43-1* strains was measured by propidium iodide staining and FACS. Line plot represents the local regression curves for the average survival of each strain ( $n > 10$ ) at different time points. Each survival curve also displays a 95% confidence interval band. Bar plot depicts the average area under the curve of each strain, and error bars represent SD. Significant differences between deletion strains and wild type, and *lon1Δ* and *yta12Δ* mutants versus *lon1Δ atg43-1* and *yta12Δ atg43-1*, respectively, were determined by two-sided *t*-test (\*  $p < 0.05$ , \*\*  $p < 0.01$ , \*\*\*  $p < 0.001$ ).

**Additional file 10.** Western blots.

**Additional file 11: Table S4.** Yeast strains used in this study.

### Acknowledgements

We thank Li-Lin Du for providing strains, members of Pombase ([www.pombase.org](http://www.pombase.org)) for the access to annotations and data sets, members from CRG/UFP Flow Cytometry Unit for their support, and José Ayté, Susanna Boron, and the rest of the Oxidative Stress and Cell Cycle group for helpful discussions.

### Authors' contributions

MV, LC, and YW performed most experiments. MV, DC, YH, EH, and MC analyzed the data. MC wrote the manuscript. The authors read and approved the final manuscript.

### Funding

This work is part of the projects PGC2018-093920-B-I00 to E.H. and BFU2016-75116-P to M.C. funded by MCIN/AEI/10.13039/501100011033 and FEDER/UE "Una Manera de hacer Europa". The Oxidative Stress and Cell Cycle group is also supported by Generalitat de Catalunya (Spain) (2017-SGR-539) and by Unidad de Excelencia María de Maeztu from MINECO (Spain) (MDM-2014-0370). M.C. is funded by the Ramon y Cajal program (MINECO-RYC2013-12858). E.H. is recipient of an ICREA Academia Award (Generalitat de Catalunya, Spain). Work in Huang's lab was supported by the National Natural Science Foundation of China (Grant 31770810 to Y.H.).

### Availability of data and materials

All images included in the main and supplementary figures are available as Mendeley dataset (<https://data.mendeley.com/datasets/98nyhrfvz/draft?m=49e13fe8-24b8-45bc-a6c8-94da5b70615c>). Materials are available from the corresponding author on request.

### Declarations

#### Ethics approval and consent to participate

Not applicable.

#### Consent for publication

Not applicable.

#### Competing interests

The authors declare no competing interests.

#### Author details

<sup>1</sup>Oxidative Stress and Cell Cycle Group, Universitat Pompeu Fabra, C/ Dr. Aiguader 88, 08003 Barcelona, Spain. <sup>2</sup>BatchX Inc, San Jose, CA, USA. <sup>3</sup>Jiangsu Key Laboratory for Microbes and Genomics, School of Life Sciences, Nanjing Normal University, 1 Wenyuan Road, Nanjing 210023, China. <sup>4</sup>Department of Biology, Geology, Physics and Inorganic Chemistry, Rey Juan Carlos University, C/ Tulipán s/n, 28933 Móstoles, Madrid, Spain.

Received: 11 January 2022 Accepted: 15 June 2022

Published online: 12 July 2022

### References

- López-Otín C, Blasco MA, Partridge L, Serrano M, Kroemer G. The hallmarks of aging. *Cell*. 2013;153:1194–217.
- Fontana L, Partridge L, Longo VD. Dietary restriction, growth factors and aging: from yeast to humans. *Science*. 2010;328:321–6.
- Kaeberlein M. Regulation of yeast replicative life span by TOR and Sch9 in response to nutrients. *Science*. 2005;310:1193–6.
- Wei M, Kim SK, Fabrizio P, Hu J, Ge H, Cheng C, et al. Life span extension by calorie restriction depends on Rim15 and transcription factors downstream of Ras/PKA, Tor, and Sch9. *Plos Genet*. 2008;4:e13–e11.
- Zuin A, Carmona Mercè, Morales-Ivorra I, Gabrielli N, Vivancos AP, Ayté J, et al. Lifespan extension by calorie restriction relies on the Sty1 MAP kinase stress pathway. *Embo J*. 2010;29:981–91.
- Alvers AL, Wood MS, Hu D, Kaywell AC Jr, WAD, Aris JP. Autophagy is required for extension of yeast chronological life span by rapamycin. *Autophagy*. 2014;5:847–9.
- Longo VD, Shadel GS, Kaeberlein M, Kennedy B. Replicative and chronological aging in *Saccharomyces cerevisiae*. *Cell Metab*. 2012;16:18–31.
- Kaeberlein M. Lessons on longevity from budding yeast. *Nature*. 2010;464:513–9.
- Lippuner AD, Julou T, Barral Y. Budding yeast as a model organism to study the effects of age. *Fems Microbiol Rev*. 2014;38:300–25.
- Zuin A, Gabrielli N, Calvo IA, García-Santamarina S, Hoe K-L, Kim DU, et al. Mitochondrial dysfunction increases oxidative stress and decreases chronological life span in fission yeast. *PLoS ONE*. 2008;3:e2842.
- Mutoh N, Kitajima S. Accelerated chronological aging of a mutant fission yeast deficient in both glutathione and superoxide dismutase having Cu and Zn as cofactors and its enhancement by Sir2 deficiency. *Biosci Biotechnology Biochem*. 2007;71:2841–4.
- Voos W, Jaworek W, Wilkening A, Bruderek M. Protein quality control at the mitochondrion. *Essays Biochem*. 2016;60:213–25.
- Dunn CD, Walter P, Tamura Y, Sesaki H, Jensen RE. Mgr3p and Mgr1p are adaptors for the mitochondrial i-AAA protease complex. *Mol Biol Cell*. 2008;19:5387–97.
- Hughes AL, Gottschling DE. An early age increase in vacuolar pH limits mitochondrial function and lifespan in yeast. *Nature*. 2013;492:261–5.
- Fehrmann S, Paoletti C, Goulev Y, Ungureanu A, Aguilaniu H, Charvin G. Aging yeast cells undergo a sharp entry into senescence unrelated to the loss of mitochondrial membrane potential. *Cell Rep*. 2013;5:1589–99.
- Stephan J, Franke J, Ehrenhofer-Murray AE. Chemical genetic screen in fission yeast reveals roles for vacuolar acidification, mitochondrial fission, and cellular GMP levels in lifespan extension. *Aging Cell*. 2013;12:574–83.
- Scheckhuber CQ, Erjavec N, Tinazli A, Hamann A, Nystrom T, Osiewacz HD. Reducing mitochondrial fission results in increased life span and fitness of two fungal ageing models. *Nat Cell Biol*. 2007;9:99–105.
- Scheckhuber CQ, Wanger RA, Mignat CA, Osiewacz HD. Unopposed mitochondrial fission leads to severe lifespan shortening. *Cell Cycle*. 2011;10:3105–10.
- Bernhardt D, Müller M, Reichert AS, Osiewacz HD. Simultaneous impairment of mitochondrial fission and fusion reduces mitophagy and shortens replicative lifespan. *Sci Rep-uk*. 2015;5:503–9.
- Wang K, Klionsky DJ. Mitochondria removal by autophagy. *Autophagy*. 2014;7:297–300.
- Kanki T, Wang K, Cao Y, Baba M, Klionsky DJ. Atg32 is a mitochondrial protein that confers selectivity during mitophagy. *Dev Cell*. 2009;17:98–109.
- Zhao D, Liu X-M, Yu Z-Q, Sun L-L, Xiong X, Dong M-Q, et al. Atg20- and Atg24-family proteins promote organelle autophagy in fission yeast. *J Cell Sci*. 2016;129:4289–304.
- Fukuda T, Ebi Y, Saigusa T, Furukawa K, Yamashita S, Inoue K, et al. Atg43 tethers isolation membranes to mitochondria to promote starvation-induced mitophagy in fission yeast. *Elife*. 2020;9:3206–29.
- Ocampo A, Barrientos A. Quick and reliable assessment of chronological life span in yeast cell populations by flow cytometry. *Mech Ageing Dev*. 2011;132:315–23.
- Roux AE, Quissac A, Chartrand P, Ferbeyre G, Rokeach LA. Regulation of chronological aging in *Schizosaccharomyces pombe* by the protein kinases Pka1 and Sck2. *Aging Cell*. 2006;5:345–57.
- Harbauer AB, Zahedi RP, Sickmann A, Pfanner N, Meisinger C. The protein import machinery of mitochondria—a regulatory hub in metabolism, stress, and disease. *Cell Metab*. 2014;19:357–72.

27. Pak VV, Ezerija D, Lyubinskaya OG, Pedre B, Tyurin-Kuzmin PA, Mishina NM, et al. Ultrasensitive genetically encoded indicator for hydrogen peroxide identifies roles for the oxidant in cell migration and mitochondrial function. *Cell Metab.* 2020;31:642–653.e6.
28. de Cubas L, Pak VV, Belousov VV, Ayté J, Hidalgo E. The mitochondria-to-cytosol H<sub>2</sub>O<sub>2</sub> gradient is caused by peroxiredoxin-dependent cytosolic scavenging. *Antioxidants.* 2021;10:731.
29. van der Blik AM, Shen Q, Kawajiri S. Mechanisms of mitochondrial fission and fusion. *Csh Perspect Biol.* 2013;5:a011072–a011072.
30. Rabl R, Soubannier V, Scholz R, Vogel F, Mendl N, Vasiljev-Neumeyer A, et al. Formation of cristae and crista junctions in mitochondria depends on antagonism between Fc1 and Su e/g. *J Cell Biol.* 2009;185:1047–63.
31. Rana A, Oliveira MP, Khamoui AV, Aparicio R, Rera M, Rossiter HB, et al. Promoting Drp1-mediated mitochondrial fission in midlife prolongs healthy lifespan of *Drosophila melanogaster*. *Nat Commun.* 2017;8:448.
32. Valente AJ, Maddalena LA, Robb EL, Moradi F, Stuart JA. A simple ImageJ macro tool for analyzing mitochondrial network morphology in mammalian cell culture. *Acta Histochem.* 2017;119:315–26.
33. Palikaras K, Lionaki E, Tavernarakis N. Coordination of mitophagy and mitochondrial biogenesis during ageing in *C. elegans*. *Nature.* 2015;521:525–8.
34. Schiavi A, Maglioni S, Palikaras K, Shaik A, Strappazzon F, Brinkmann V, et al. Iron-starvation-induced mitophagy mediates lifespan extension upon mitochondrial stress in *C. elegans*. *Curr Biol.* 2015;25:1810–22.
35. Richard VR, Leonov A, Beach A, Burstein MT, Koupaki O, Gomez-Perez A, et al. Macromitophagy is a longevity assurance process that in chronologically aging yeast limited in calorie supply sustains functional mitochondria and maintains cellular lipid homeostasis. *Aging.* 2013;5:234–69.
36. Ocampo A, Liu J, Schroeder EA, Shadel GS, Barrientos A. Mitochondrial respiratory thresholds regulate yeast chronological life span and its extension by caloric restriction. *Cell Metab.* 2012;16:55–67.
37. Kwon Y-Y, Choi K-M, Cho C, Lee C-K. Mitochondrial efficiency-dependent viability of *Saccharomyces cerevisiae* mutants carrying individual electron transport chain component deletions. *Mol Cells.* 2015;38:1054–63.
38. Hacıoğlu E, Demir AB, Koc A. Identification of respiratory chain gene mutations that shorten replicative life span in yeast. *Exp Gerontol.* 2012;47:149–53.
39. Li W, Sun L, Liang Q, Wang J, Mo W, Zhou B. Yeast AMID homologue Ndi1p displays respiration-restricted apoptotic activity and is involved in chronological aging. *Mol Biol Cell.* 2006;17:1802–11.
40. Lee S-J, Hwang AB, Kenyon C. Inhibition of respiration extends *C. elegans* life span via reactive oxygen species that increase HIF-1 activity. *Curr Biol.* 2010;20:2131–6.
41. Labbadia J, Briemann RM, Neto MF, Lin Y-F, Haynes CM, Morimoto RI. Mitochondrial stress restores the heat shock response and prevents proteostasis collapse during aging. *Cell Rep.* 2017;21:1481–94.
42. Tavallaie M, Voshtani R, Deng X, Qiao Y, Jiang F, Collman JP, et al. Moderation of mitochondrial respiration mitigates metabolic syndrome of aging. *Proc Natl Acad Sci.* 2020;117:9840–50.
43. Wagner I, Artl H, van Dyck L, Langer T, Neupert W. Molecular chaperones cooperate with PIM1 protease in the degradation of misfolded proteins in mitochondria. *Embo J.* 1994;13:5135–45.
44. Savelev AS, Novikova LA, Kovaleva IE, Luzikov VN, Neupert W, Langer T. ATP-dependent proteolysis in mitochondria. m-AAA protease and PIM1 protease exert overlapping substrate specificities and cooperate with the mtHsp70 system. *J Biol Chem.* 1998;273:20596–602.
45. Bota DA, Davies KJA. Lon protease preferentially degrades oxidized mitochondrial aconitase by an ATP-stimulated mechanism. *Nat Cell Biol.* 2002;4:674–80.
46. Erjavec N, Bayot A, Gareil M, Camougrand N, Nystrom T, Friguet B, et al. Deletion of the mitochondrial Pim1/Lon protease in yeast results in accelerated aging and impairment of the proteasome. *Free Radical Bio Med.* 2013;56:9–16.
47. Luce K, Osiewicz HD. Increasing organismal healthspan by enhancing mitochondrial protein quality control. *Nat Cell Biol.* 2009;11:852–8.
48. Wang Y, Yan J, Zhang Q, Ma X, Zhang J, Su M, et al. The Schizosaccharomyces pombe PPR protein Ppr10 associates with a novel protein Mpa1 and acts as a mitochondrial translational activator. *Nucleic Acids Res.* 2017;45:3323–40.
49. Matsushima Y, Goto Y, Kaguni LS. Mitochondrial Lon protease regulates mitochondrial DNA copy number and transcription by selective degradation of mitochondrial transcription factor A (TFAM). *Proc Natl Acad Sci.* 2010;107:18410–5.
50. Nolden M, Ehses S, Koppen M, Bernacchia A, Rugarli E, Langer T. The m-AAA protease defective in hereditary spastic paraplegia controls ribosome assembly in mitochondria. *Cell.* 2005;123:277–89.
51. Guha S, López-Maury L, Shaw M, Bähler J, Norbury CJ, Agashe VR. Transcriptional and cellular responses to defective mitochondrial proteolysis in fission yeast. *J Mol Biol.* 2011;408:222–37.
52. Schulz TJ, Zarse K, Voigt A, Urban N, Birringer M, Ristow M. Glucose restriction extends *Caenorhabditis elegans* life span by inducing mitochondrial respiration and increasing oxidative stress. *Cell Metab.* 2007;6:280–93.
53. Roux AE, Dutcher SK, Leroux A, Alaamery MA, Hoffman CS, Chartrand P, et al. Pro-aging effects of glucose signaling through a G protein-coupled glucose receptor in fission yeast. *Plos Genet.* 2009;5:e1000408–17.
54. Kaya A, Phua CZJ, Lee M, Wang L, Tyshkovskiy A, Ma S, et al. Evolution of natural lifespan variation and molecular strategies of extended lifespan in yeast. *Elife.* 2021;10:e64860.
55. Lin Y, Lu J, Zhang J, Walter W, Dang W, Wan J, et al. Protein acetylation microarray reveals that NuA4 controls key metabolic target regulating gluconeogenesis. *Cell.* 2009;136:1073–84.
56. Fabrizio P, Gattazzo C, Battistella L, Wei M, Cheng C, McGrew K, et al. Sir2 blocks extreme life-span extension. *Cell.* 2005;123:655–67.
57. Casatta N, Porro A, Orlandi I, Brambilla L, Vai M. Lack of Sir2 increases acetate consumption and decreases extracellular pro-aging factors. *Biochimica Et Biophysica Acta Bba - Mol Cell Res.* 2013;1833:593–601.
58. Orlandi I, Coppola DP, Strippoli M, Ronzulli R, Vai M. Nicotinamide supplementation phenocopies SIR2 inactivation by modulating carbon metabolism and respiration during yeast chronological aging. *Mech Ageing Dev.* 2017;161:277–87.
59. Yuan Y, Cruzat VF, Newsholme P, Cheng J, Chen Y, Lu Y. Regulation of SIRT1 in aging: roles in mitochondrial function and biogenesis. *Mech Ageing Dev.* 2016;155:10–21.
60. Pereira C, Costa V, Martins LM, Saraiva L. A yeast model of the Parkinson's disease-associated protein Parkin. *Exp Cell Res.* 2015;333:73–9.
61. Wang K, Jin M, Liu X, Klionsky DJ. Proteolytic processing of Atg32 by the mitochondrial f-AAA protease Yme1 regulates mitophagy. *Autophagy.* 2014;9:1828–36.
62. Alfa C, Fantes P, Hyams J, McLeod M, Warbrick E. Experiments with Fission Yeast: A Laboratory Course Manual. Cold Spring Harbor: Cold Spring Harbor Laboratory; 1993.
63. Murakami C, Kaerberlein M. Quantifying yeast chronological life span by outgrowth of aged cells. *J Vis Exp Jove.* 2009;27:e1156.
64. Zhou Y, Zhou B, Pache L, Chang M, Khodabakhshi AH, Tanaseichuk O, et al. Metascape provides a biologist-oriented resource for the analysis of systems-level datasets. *Nat Commun.* 2019;10(1):1523.
65. Schindelin J, Arganda-Carreras I, Frise E, Kaynig V, Longair M, Pietzsch T, et al. Fiji: an open-source platform for biological-image analysis. *Nat Methods.* 2012;9:676–82.
66. Vivancos AP, Castillo EA, Biteau B, Nicot C, Ayté J, Toledano MB, et al. A cysteine-sulfenic acid in peroxiredoxin regulates H<sub>2</sub>O<sub>2</sub>-sensing by the antioxidant Pap1 pathway. *Proc Natl Acad Sci.* 2005;102:8875–80.
67. Jara M, Fox T, Vivancos AP, Calvo IA, Moldón A, Sansó M, et al. The peroxiredoxin Tpx1 is essential as a H<sub>2</sub>O<sub>2</sub> scavenger during aerobic growth in fission yeast. *Mol Biol Cell.* 2007;18:2288–95.
68. Chiron S, Gaisne M, Guillou E, Belenguer P, Clark-Walker GD, Bonnefoy N. Studying mitochondria in an attractive model: *Schizosaccharomyces pombe*. *Methods Mol Biol.* 2007;372:91–105.

## Publisher's Note

Springer Nature remains neutral with regard to jurisdictional claims in published maps and institutional affiliations.

Ready to submit your research? Choose BMC and benefit from:

- fast, convenient online submission
- thorough peer review by experienced researchers in your field
- rapid publication on acceptance
- support for research data, including large and complex data types
- gold Open Access which fosters wider collaboration and increased citations
- maximum visibility for your research: over 100M website views per year

At BMC, research is always in progress.

Learn more [biomedcentral.com/submissions](https://biomedcentral.com/submissions)

